Supporting Information

In-Situ Electrochemical Synthesis of Superhydrophilic NiCoMn Trimetallic-alloy Nanosheets via Dynamic Hydrogen Bubble Template Method for Developing High Current Density Hydrogen Production Electrocatalyst

Shahab Paygozar[a], Alireza Sabour Rouhaghdam[a], Abdolvahab Seif [b], Ghasem Barati Darband[c]*

a- Department of Materials Engineering, Faculty of Engineering, Tarbiat Modares University, P.O. Box: 14115-143, Tehran, Iran
b- Dipartimento di Fisica e Astronomia "G. Galilei", Università di Padova, via Marzolo 8, Padova I-35131, Italy
c- Materials and Metallurgical Engineering Department, Faculty of Engineering, Ferdowsi University of Mashhad, Mashhad 91775-1111, Iran

Corresponding Author

E-mail: baratidarband@um.ac.ir (Ghasem Barati Darband)

Experimental procedures

Preparation of the NiCoMn/NF electrocatalyst

The NiCoMn electrocatalyst was fabricated through the dynamic hydrogen bubble template (DHBT) approach. Nickel foam with the dimension of 1 × 1 cm^2 served as the substrate for the electrodeposition of NiCoMn. Firstly, and before the electrodeposition process, the nickel foam was prepared for 15 minutes in acetone for degreasing, and then for 25 seconds in a 2 M HCl solution with ultrasonic assistance. Finally, the nickel foam was washed with distilled water and dried at room temperature. The electrochemical electrodeposition process was carried out in a two-electrode system, including a platinum electrode (anode) and a working electrode (cathode), using the DHBT technique with a power source device and at room temperature with a pH of 2.5. The electrodeposition bath contained 0.1 M $NiCl_2.6H_2O$ (source of nickel ions), 0.1 M $CoCl_2.6H_2O$ (source of cobalt ions), 0.1 M $MnCl_2.4H_2O$ (source of manganese ions), and 2 M NH_4Cl to adjust the pH of the bath. Furthermore, control electrodes of NiCo and NiMn were also produced using an analogous electrochemical electrodeposition technique to that of NiCoMn, employing their respective precursor solutions on the nickel foam substrate. Finally, to optimize the sample, a comparison of LSV and EIS curves was used for the synthesized samples among the electrodeposition current densities of -1, -3, and -5 $A.cm^{-2}$, and electrodeposition duration of 5, 10, 30, and 60 seconds. The sample synthesized at a current density of -3 $A.cm^{-2}$ and a duration of 60 seconds was selected as the optimized sample.

Materials characterization

A field emission scanning electron microscope (FE-SEM TESCAN MIRA3 equipped with a chemical composition analyzer and elemental map) was used to examine the morphology and microstructure of the electrodes, and energy dispersive X-ray spectroscopy (EDS) was used to examine the map and elemental compositions more precisely. Transmission electron microscope (TEM) images were prepared using a Twin Super 20F 2G Tecnai FEI device. Also, to know the crystalline or amorphous nature and to identify the crystalline structures of the coating, X-ray diffraction (XRD) analysis with a scanning rate of 0.02 °/s was performed using a model device (Bruker AXS D8 ADVANCE and with CuKα radiation λ=1.5406 A°) and was performed with an angle of 2θ in the range between 5 and 80 degrees. The bubble contact angle on the nickel foam and NiCoMn/NF electrode was measured by placing a drop of 1.0 M KOH according to the instructions specified in standard D7334. Next, by fixing the drops on the electrode surface after a period of 25 seconds, the contact angle was measured. It should be mentioned that the ZHIKAN model CAG-20 device was used for contact angle analysis.

Electrochemical properties

A standard three-electrode cell was used to perform electrochemical tests. In this cell, Ag/AgCl was used as a reference electrode, and graphite rod and synthesized electrodes were used as counter and working electrodes. Also, all electrochemical tests were performed with a Bio-Logic SP-300 potentiostat device and in 1 M KOH solution. The electrocatalytic activity of the samples for HER was investigated using linear sweep voltammetry (LSV) with a scan rate of 5.0 $mV.s^{-1}$, up to a high current density (-1000 $mA.cm^{-2}$). In addition, the Tafel slopes extracted from LSV curves and

electrochemical impedance spectroscopy (EIS) tests in the frequency range of 100 kHz to 100 MHz were evaluated to investigate hydrogen evolution kinetics and charge transfer resistance for the synthesized electrodes. Cyclic voltammetry (CV) test at different scan rates between 10 and 120 mV.dec^{-1} was used to calculate the electrical double layer capacity (Cdl), electrochemical surface area (ECSA), and surface roughness factor (RF). Evaluation of the long-term durability of NiCoMn electrode compared to HER in Cathodic extreme conditions (-500 mA.cm^{-2}) and evaluation of the durability during overall water splitting (100 mA.cm^{-2}) by chronopotentiometry test for 150 hours and step chronopotentiometry at ten levels of current density from -50 to -500 mA.cm^{-2} (duration of each level 900 seconds) for HER in 1 M KOH solution was done. Also, for further evaluation, the stability of the NiCoMn electrocatalyst was investigated after 3000 CV cycles in the potential range of 0 to -0.3 V with a scan rate of 100 mV s^{-1}. In addition, for a more accurate evaluation of the surface using the dynamic specific resistance test of the separation of hydrogen bubbles produced during HER for 240 seconds with a frequency of 10 Hz and a potential of -0.2 V vs. RHE to evaluate the super-aerobic property of the electrode. NiCoMn/NF and its comparison with platinum foil was done in 1 M KOH solution. The amount of hydrogen and oxygen gas produced by gas chromatography (Bruker GC450) at a current density of 50 mA.cm^{-2} for the NiCoMn/NF||NiCoMn/NF couple was measured based on i-t values every ten minutes and for one hour.

$$FE_{H2} = \frac{2 \times 96485 \times nH2}{QHER} \quad (1)$$

$$n_{H2} = \frac{VH2}{Vm} \quad (2)$$

$$FE_{O2} = \frac{2 \times 96485 \times nO2}{QOER} \quad (3)$$

$$n_{O2} = \frac{VO2}{Vm} \quad (4)$$

In this regard, Q is the total charge distributed in the electrocatalyst, V comprises the gas volume obtained from gas chromatography, Vm denotes the molar volume (22.4 L.mol^{-1}), and n is the produced gas molar mass.

In addition, all the potentials reported in this research are reported using the following formula based on the reversible hydrogen electrode (RHE).

$$V_{RHE} = V \text{ (vs. Ag/AgCl)} + V° \text{ Ag/AgCl} + 0.059 \text{ pH} \quad (5)$$

Calculation detail of double-layer capacitance (Cdl), electrochemical surface area (ECSA), and roughness factor (RF)

The Cdl values of prepared samples were calculated using CV curves. Therefore, CV tests were carried out in the non-faradic potentials zone (0.75 to 0.85 V vs. Ag/AgCl) at different scan rates. ECSA and RF values are calculated using the following equations.

$$\text{ECSA} = \frac{c_{dl}}{c_s} \quad (6)$$

Where Cs denotes the capacitance of a flat surface (20 μF.cm^{-2}). The RF value obtained by solving equation (5):

$$\text{RF} = \frac{c_{dl}}{c_0} \quad (7)$$

Where C_0 comprises the ideal planar metal oxides capacitance (i.e., NiO) with smooth surfaces (60 μF.cm^{-2}).

Based on this, the CV test was performed at seven different scan rates including 10, 20, 40, 60, 80, 100, and 120 mV.s^{-1} in the non-faradic potential zone on the surface of different electrodes.

Turnover frequency (TOF) Calculation

Equation (8) was used to calculate the turnover frequency (TOF) of HER at a fixed overpotential by considering the surface area of the geometric substrate and the current density. These TOF values were then used to generate graphs.

$$\text{TOF} = \frac{Total\ Hydrogen\ Turn\ Overs/cm^2\ geometric\ area}{Surface\ active\ sites/cm^2\ geometric\ area} \quad (8)$$

The total number of evolved hydrogen bubbles is calculated in accordance with the current density at a given overpotential on the basis of equation (7):

$$H_2 = \left(j\frac{mA}{cm^2}\right)\left(\frac{1C.s^{-1}}{1000\ mA}\right)\left(\frac{1\ mol.e^{-1}}{96485.3\ C}\right)\left(\frac{1\ mol.H_2}{2\ mol.e^-}\right) \times \left(\frac{6.022 \times 10^{23}\ H_2\ molecules}{1\ mol\ H_2}\right) = 3.12 \times 10^{15}\ \frac{H_2}{s}\ \text{per}\frac{mA}{cm^2} \quad (9)$$

Supposing that all sites at the catalyst surfaces can participate as active centers for HER, their number is calculated as below:

$$N = \frac{\left(\frac{4\ atoms}{43.76\ \mathring{A}}\right)^{2/3}}{} = 9.01 \times 10^{14}\ atoms.cm_{real}^{-2} \quad (10)$$

$$TOF = \frac{\left(\left(3.12 \times 10^{15} \frac{\frac{H_2}{s}}{cm^2} per \frac{mA}{cm^2}\right) \times |j|\right)}{\left(9.01 \times 10^{14} atoms.cm_{real}^{-2}\right) \times A_{ECSA}} \quad (11)$$

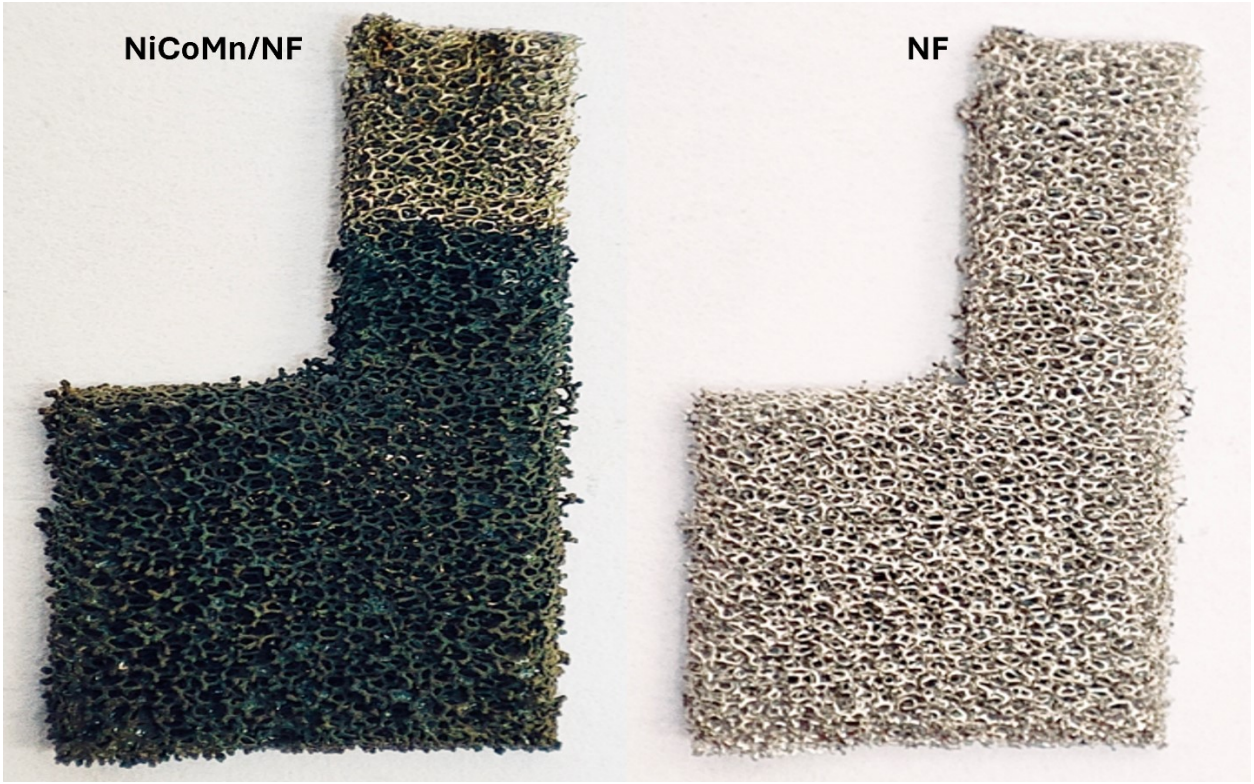

Figure. S1. Pictures of Ni foam before and after NiCoMn coating

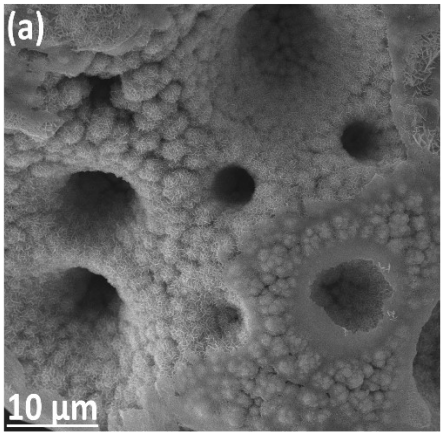

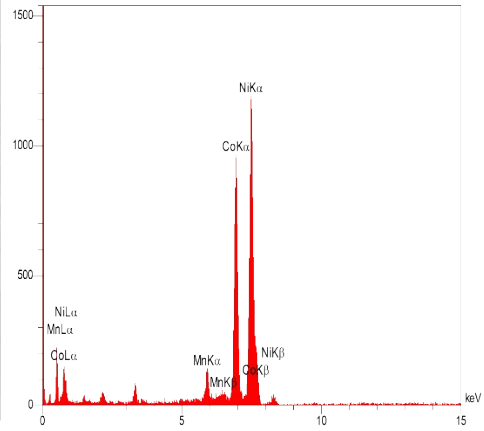

Atomic percentage

Ni	50.83%
Co	44.13%
Mn	5.04%

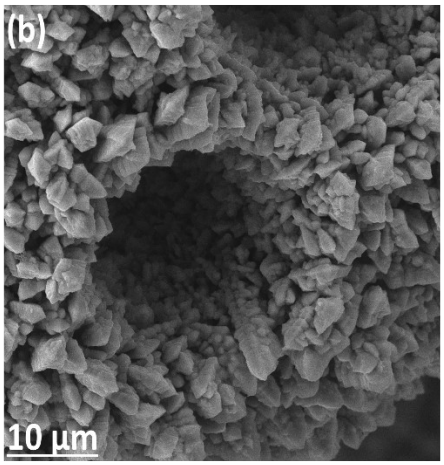

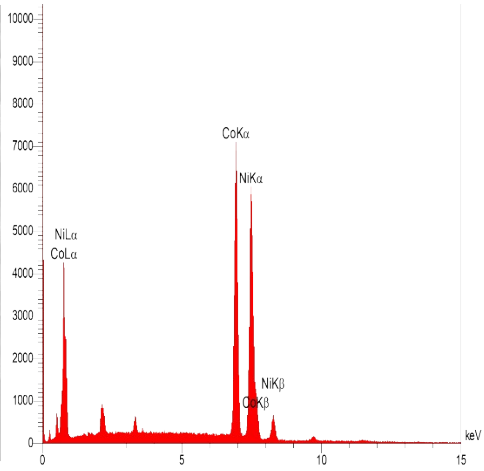

Atomic percentage

Ni	46.83%
Co	53.17%

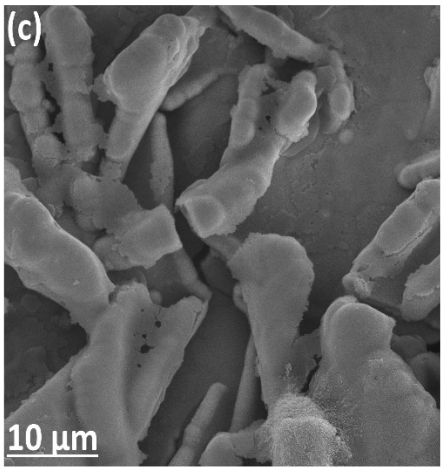

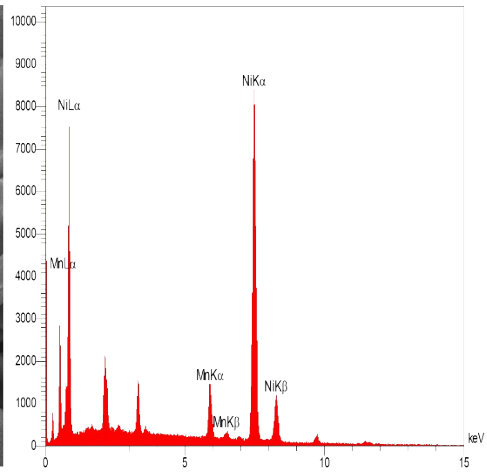

Atomic percentage

Ni	89.48%
Mn	10.52%

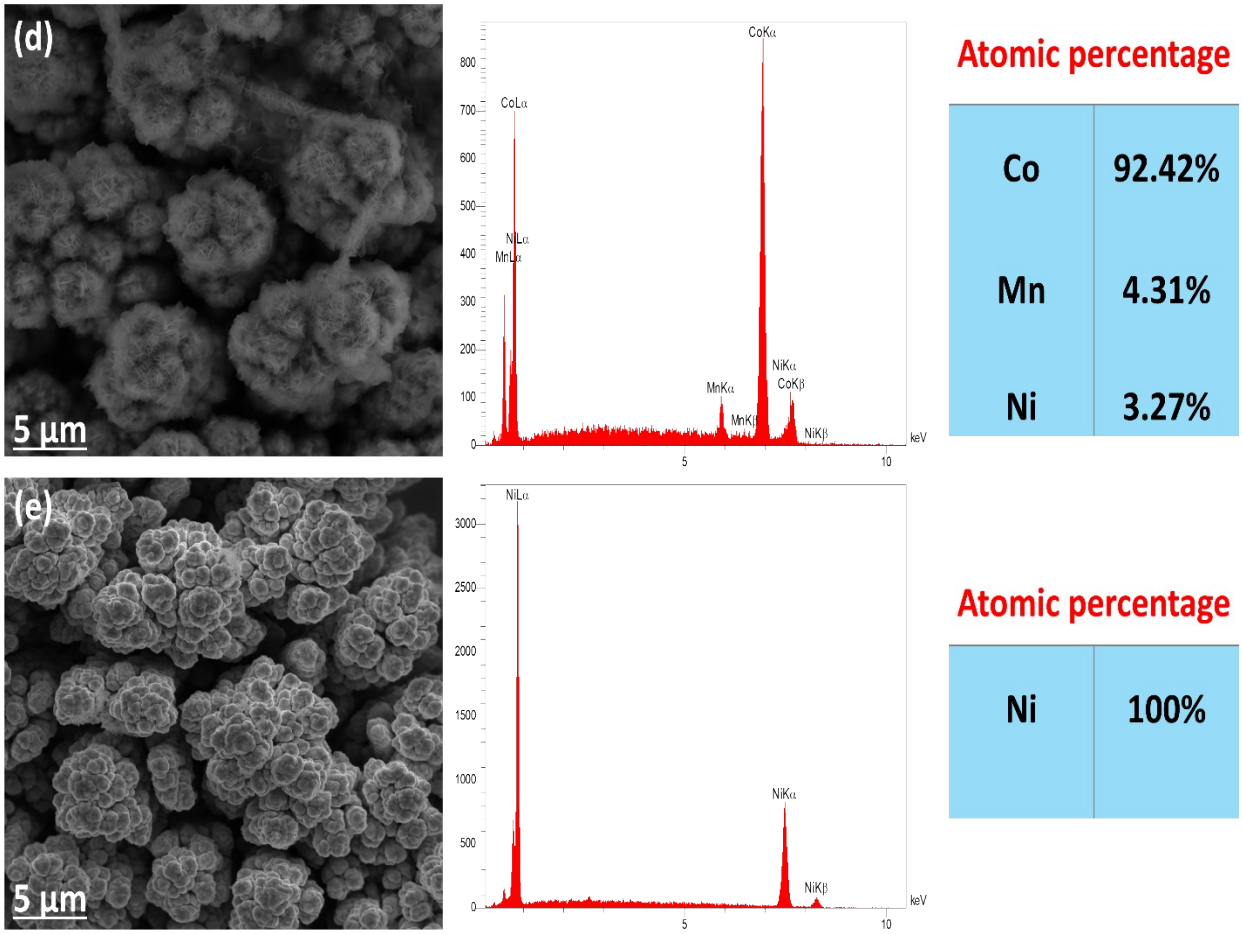

Figure. S2. FE-SEM images and EDS spectra for prepared electrodes, (a) NiCoMn/NF, (b) NiCo/NF, (c) NiMn/NF, (d) CoMn/NF, and (e) Ni/NF.

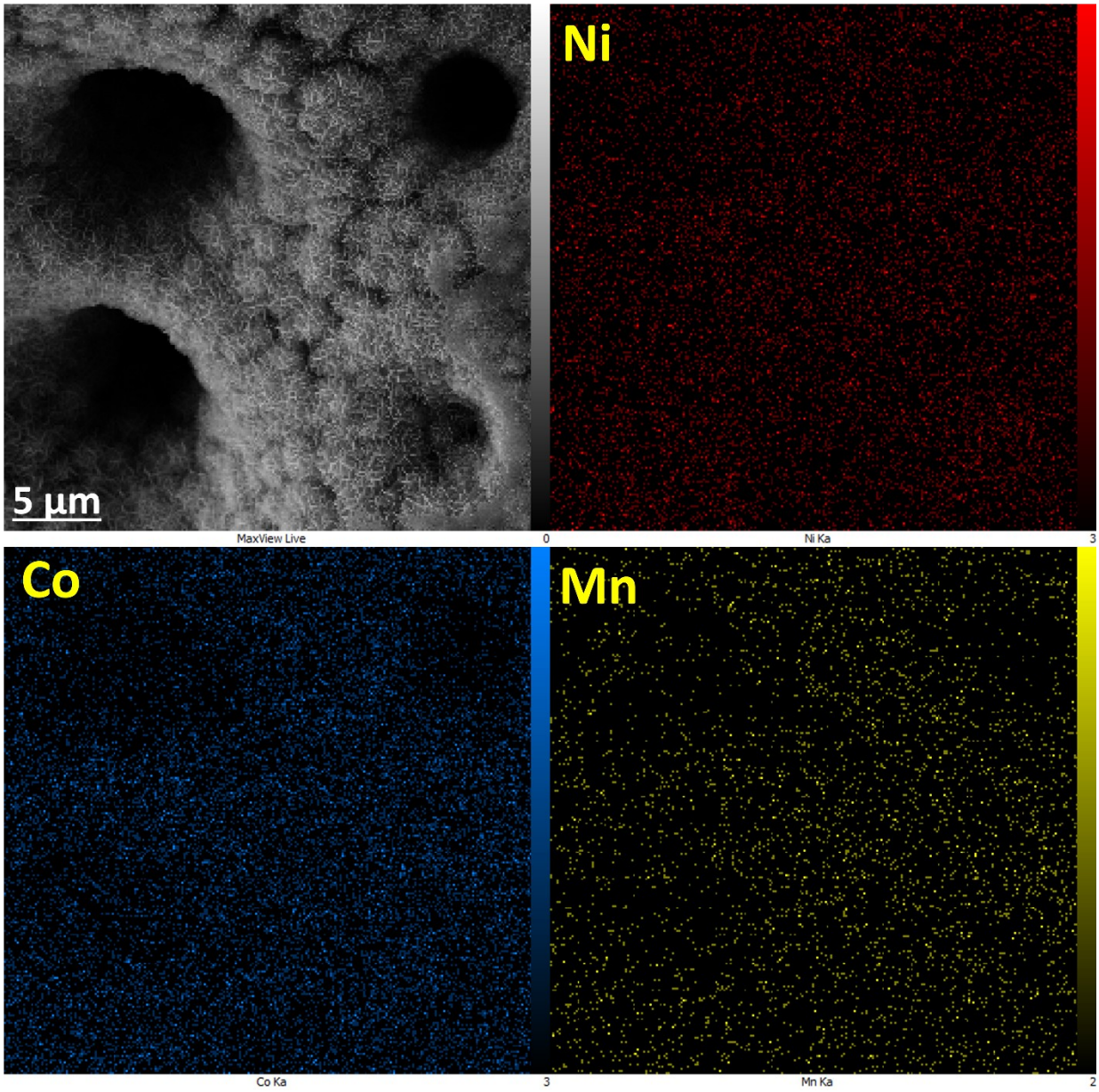

Figure. S3. EDS-elemental mapping of NiCoMn electrode, Ni (red), Co (blue), and Mn (yellow).

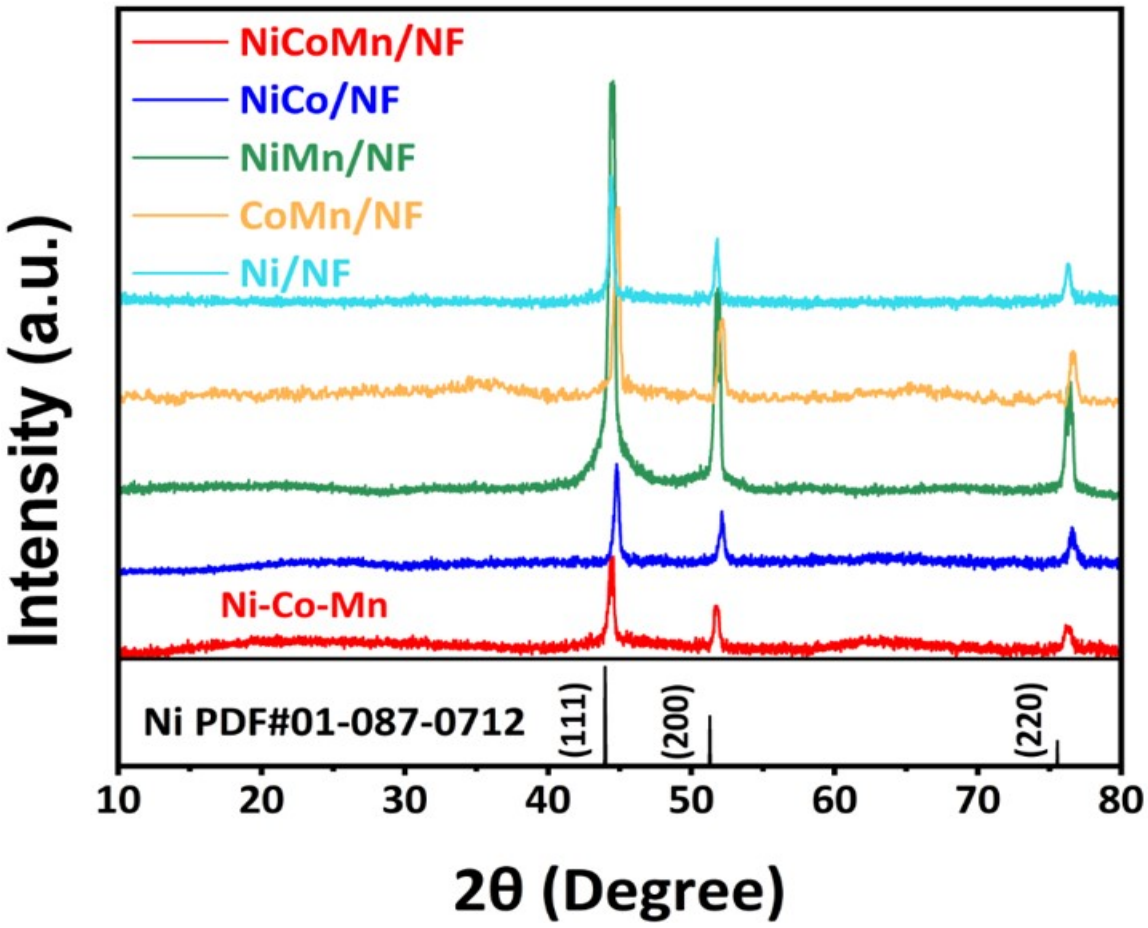

Figure. S4. XRD pattern for NiCoMn/NF, NiCo/NF, NiMn/NF, CoMn/NF, and Ni/NF electrodes.

Finding optimized NiCoMn/NF electrocatalyst

In the first step, to optimize and determine the current density of DHBT deposition on the inherent properties of the prepared samples, time was held constant at 30 s. Subsequently, linear sweep voltammetry (LSV) and electrochemical impedance spectroscopy (EIS) were performed. LSV and EIS diagrams of NiCoMn/NF samples prepared at current densities of -1, -3, and -5 $A.cm^{-2}$ are shown in **Figure S5** a and b. As can be seen, the sample prepared at a current density of -3 $A.cm^{-2}$ exhibits the best hydrogen evolution reaction (HER) performance, with overpotentials of -61 and -160 mV at current densities of -10 and -100 $mA.cm^{-2}$, respectively, and the lowest charge transfer resistance (2.67 $\Omega.cm^2$). In the second step, with the synthesis current density determined (-3 $A.cm^{-2}$), optimization of different deposition times was conducted. LSV and EIS diagrams of NiCoMn/NF samples prepared at a current density of -3 $A.cm^{-2}$ and times of 5, 10, 30, and 60 s are shown in **Figure S1** c and d. The evaluation of HER performance according to Figure S1c indicates that the sample prepared in 60 s, with overpotentials of -33 and -130 mV at current densities of -10 and -100 $mA.cm^{-2}$, respectively, has the best performance compared to those prepared in 5 (-120 and -271 mV at -10 and -100 $mA.cm^{-2}$), 10 (-84 and -228 mV at -10 and -100 $mA.cm^{-2}$), and 30 s (-65 and -168 mV at -10 and -100 $mA.cm^{-2}$). Furthermore, the NiCoMn/NF

sample prepared in 60 s exhibits the smallest charge transfer resistance (0.67 Ω.cm^2) compared to the other samples prepared in 5 (5.31 Ω.cm^2), 10 (3.17 Ω.cm^2), and 30 s (2.68 Ω.cm^2). This indicates high electronic conductivity of the electrode and contributes to the highest HER performance, especially at high current densities. Due to the low overpotential of HER at different current densities and the small charge transfer resistance, the optimal NiCoMn/NF sample prepared at -3 A.cm^{-2} and 60 s was chosen as the target electrode to perform further electrochemical measurements to estimate its performance for HER.

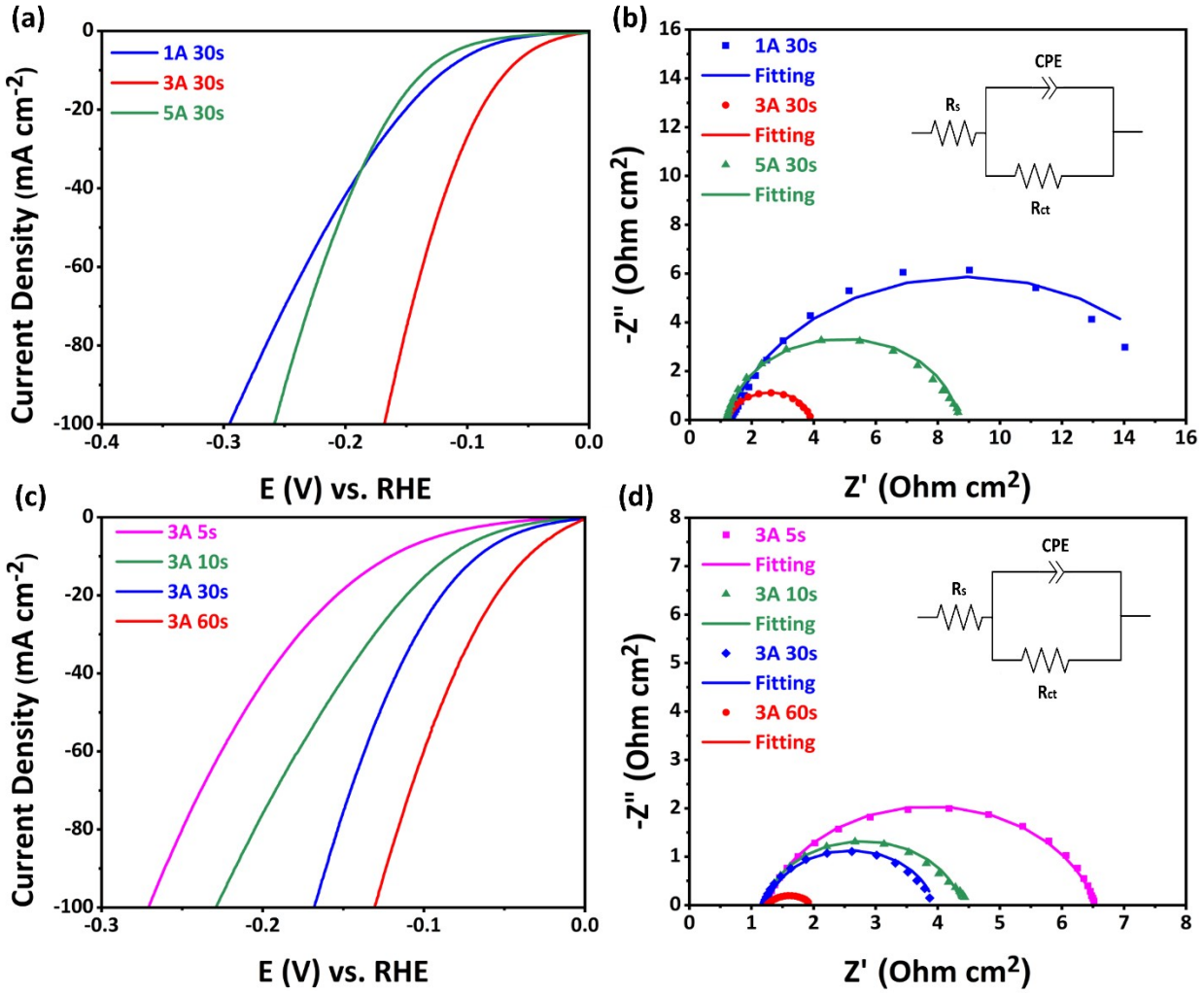

Figure. S5. Electrochemical performance for HER in 1.0 M KOH solution with current density -1, -3, and -5 A.cm^{-2} at 30 s; (b) Nyquist curves of electrodes prepared at a constant time of 30s and current densities of -1, -3, and -5 A.cm^{-2}, (c) Electrochemical performance for HER in 1.0 M KOH solution with a 3A current density at the times of 5, 10, 30, and 60 s; (d) Nyquist curves of electrodes prepared in constant current density -3 A.cm^{-2} and times of 5, 10, 30, and 60 s.

Table. S2. Comparison of catalytic parameters of NiCoMn/NF and other trimetallic-alloy electrocatalysts for HER.

Catalyst	Preparation method	Electrolyte	HER overpotential at the corresponding j (mV \\ $mA.cm^{-2}$)	Tafel slope ($mV.dec^{-1}$)	Cell voltage required at 10 $mA.cm^{-2}$ // Stability (hours)	Refs
NiCoMn/NF	Electrodeposition	1.0 M KOH	-33//-10 -242//-1000	44.2	1.43//300	This work
NiRuIr-G	Hydrothermal	0.5 M H_2SO_4	-80//-10	48	-	[1]
RuCoMn@NC	Hydrothermal	1.0 M KOH	-38//-10	34	1.63//-	[2]
NiFeMo/NF	Hydrothermal	1.0 M KOH	-45//-10	-	1.45//50	[3]
NiCuMn/NF	Electrodeposition	1.0 M KOH	-63//-10	111	1.54//24	[4]
NiFeRu-LDH	Hydrothermal	1.0 M KOH	-29//-10	31	1.52//10	[5]
$Fe_{1.0}Co_{1.1}Ni_{1.4}$–NC	Solvothermal	1.0 M KOH	-175//-10	168	1.52//20	[6]
AgAuCu	Solvothermal	0.5 M H_2SO_4	-163//-10	48	-	[7]
NCMO@NC-450	Hydrothermal	1.0 M KOH + 1.0 M CH_3OH	-220//-50	115	1.68//30	[8]
PtRhCo PAANFs	Hydrothermal	0.5 M KOH	-36//-10	48	-	[9]
$CoSe_2$@$NiSe_2$@ $MoSe_2$	Hydrothermal	1.0 M KOH	-38//-10	38	-	[10]
CoMoRu/CC	Electrodeposition	1.0 M KOH	-248//-100	120	-	[11]
Cu_2CoSnS_4	solvent	0.5 M H_2SO_4	-192//-10	98.6	-	[12]

PtNiCo HAMPs	etching	1.0 M KOH	-20//-10	46.3	-	[13]
Ni-Fe-B/NF	borothermal	1.0 M KOH	-63.5//-10	56.3	1.57	[14]
Rh-Ag-Si	Hydrothermal	0.5 M H_2SO_4	-120//-10	51	-	[15]
Rh-Au-Si	solvent	0.5 M H_2SO_4	-60//-10	24	-	[16]
PtAgCo-II	etching	0.5 M H_2SO_4	-400//-705	27	-	[17]
MnNiCo-P/NF	Electrodeposition	1.0 M KOH	-14//-10	58	1.48//50	[18]
Pt/NiCo@C	solvothermal	1.0 M KOH	-130//-10	48	-	[19]
$Pd_{58}Cu_{32}Ir_{10}$-NCs	Hydrothermal	1.0 M KOH	-54//-10	59	-	[20]
Pt_{53}- $Ru_{39}Ni_8$	-	0.5 M H_2SO_4	-37//-10	46	-	[21]
Pd/Cu-Pt	Hydrothermal	0.5 M H_2SO_4	-50//-10	25	-	[22]
$FeNi_3Mo_x$	Hydrothermal	1.0 M KOH	-112//-10	109	-	[23]
FeCoCuP@NC	Hydrothermal	1.0 M KOH 0.5 M H_2SO_4	-169//-10 -80//10	47.6 48.8	- -	[24]
NiCoCr@NF	Electrodeposition	1.0 M KOH	-11//-10	109	-	[25]

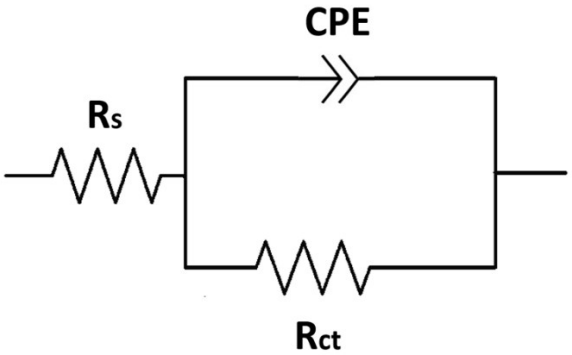

Figure. S6. Equivalent circuits are used to fit all Nyquist curves.

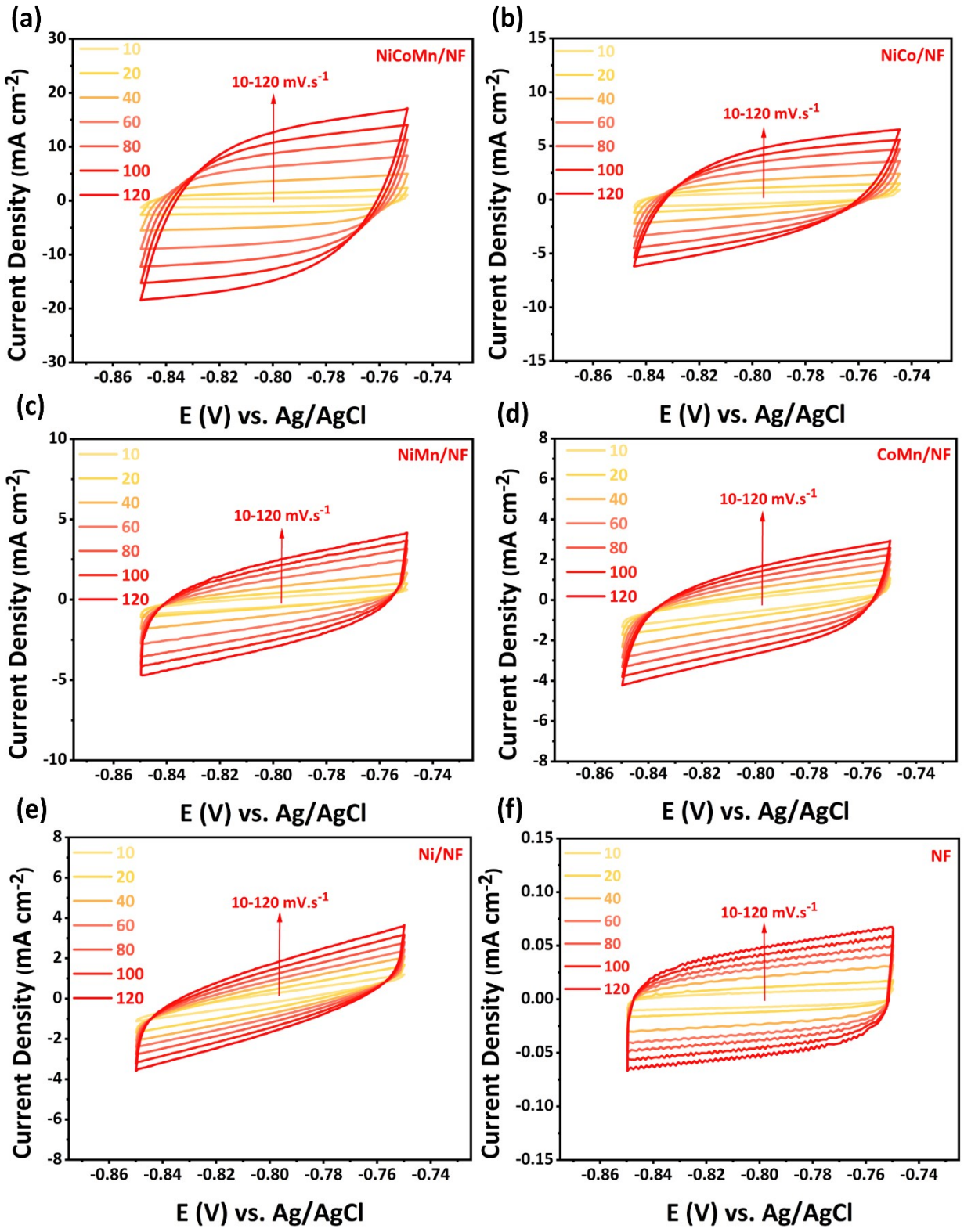

Figure. S7. CV curves for (a) NiCoMn/NF, (b) NiCo/NF, (c) NiMn/NF, (d) CoMn/NF, (e) Ni/NF, and (f) NF electrocatalysts.

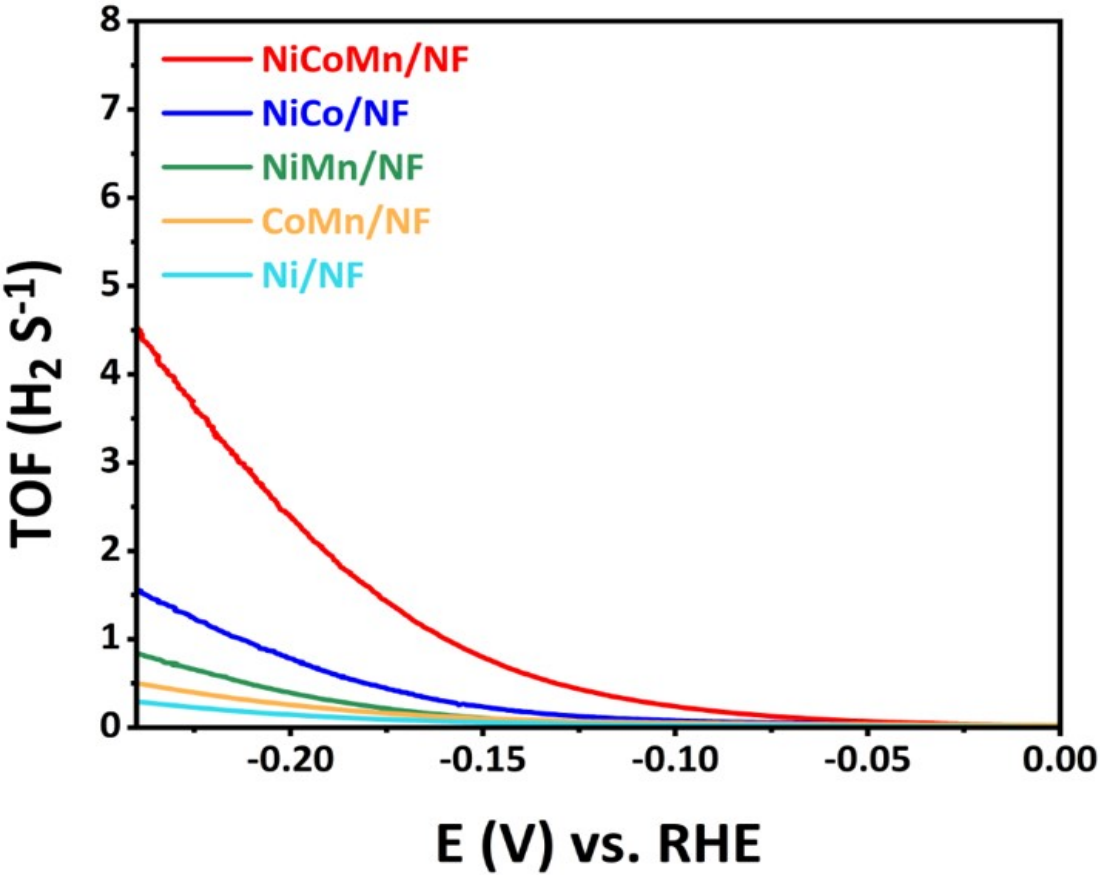

Figure. S8. TOF plots for NiCoMn/NF, NiCo/NF, NiMn/NF, CoMn/NF, and Ni/NF electrocatalyst.

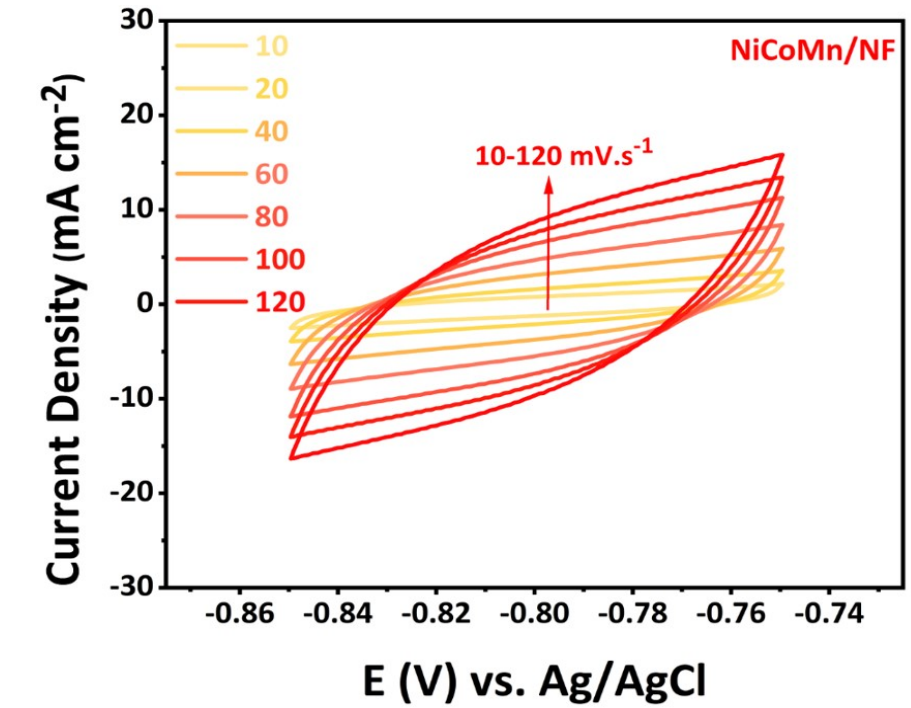

Figure. S9. CV curves at different scan rates related to NiCoMn/NF electrocatalyst after the HER stability test.

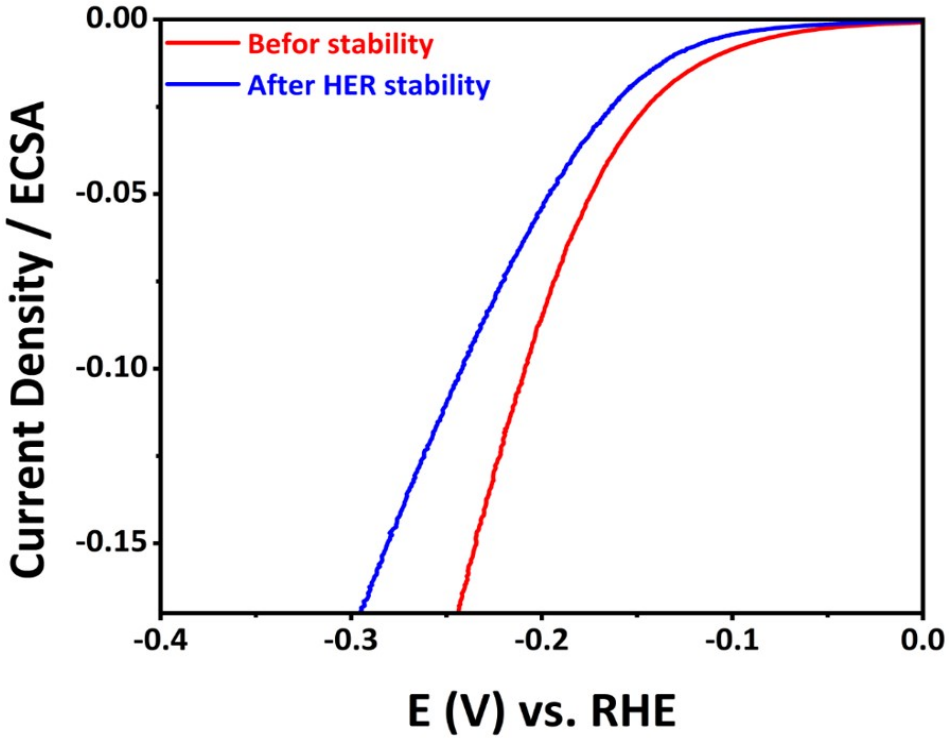

Figure. S10. CV curves at different scan rates related to NiCoMn/NF electrocatalyst after the HER stability test.

Table. S2. EIS data of different samples recorded at a potential of -1.1 V vs. Ag/AgCl (-0.0746 V vs. RHE) for HER.

samples	Rs ($\Omega.cm^2$)	CPE ($F.s^{n-1}.cm^{-2}$)	n	Rct ($\Omega.cm^2$)
NiCoMn/NF-1A 30s	1.22	0.024	0.83	15.34
NiCoMn/NF-3A 30s	1.17	0.22	0.89	2.68
NiCoMn/NF-5A 30s	1.19	0.006	0.93	7.40
NiCoMn/NF-3A 5s	1.15	0.008	0.83	5.31
NiCoMn/NF-3A 10s	1.18	0.22	0.88	3.17
NiCoMn/NF-3A 30S	1.16	0.22	0.89	2.68
NiCoMn/NF-3A 60s	1.22	0.51	0.78	0.67
NiCo/NF	1.21	0.37	0.82	3.23
NiMn/NF	1.23	0.31	0.88	3.92
CoMn/NF	1.16	0.17	0.89	6.48
Ni/NF	1.13	0.11	0.91	9.72
NF	1.26	0.0004	0.97	64.08

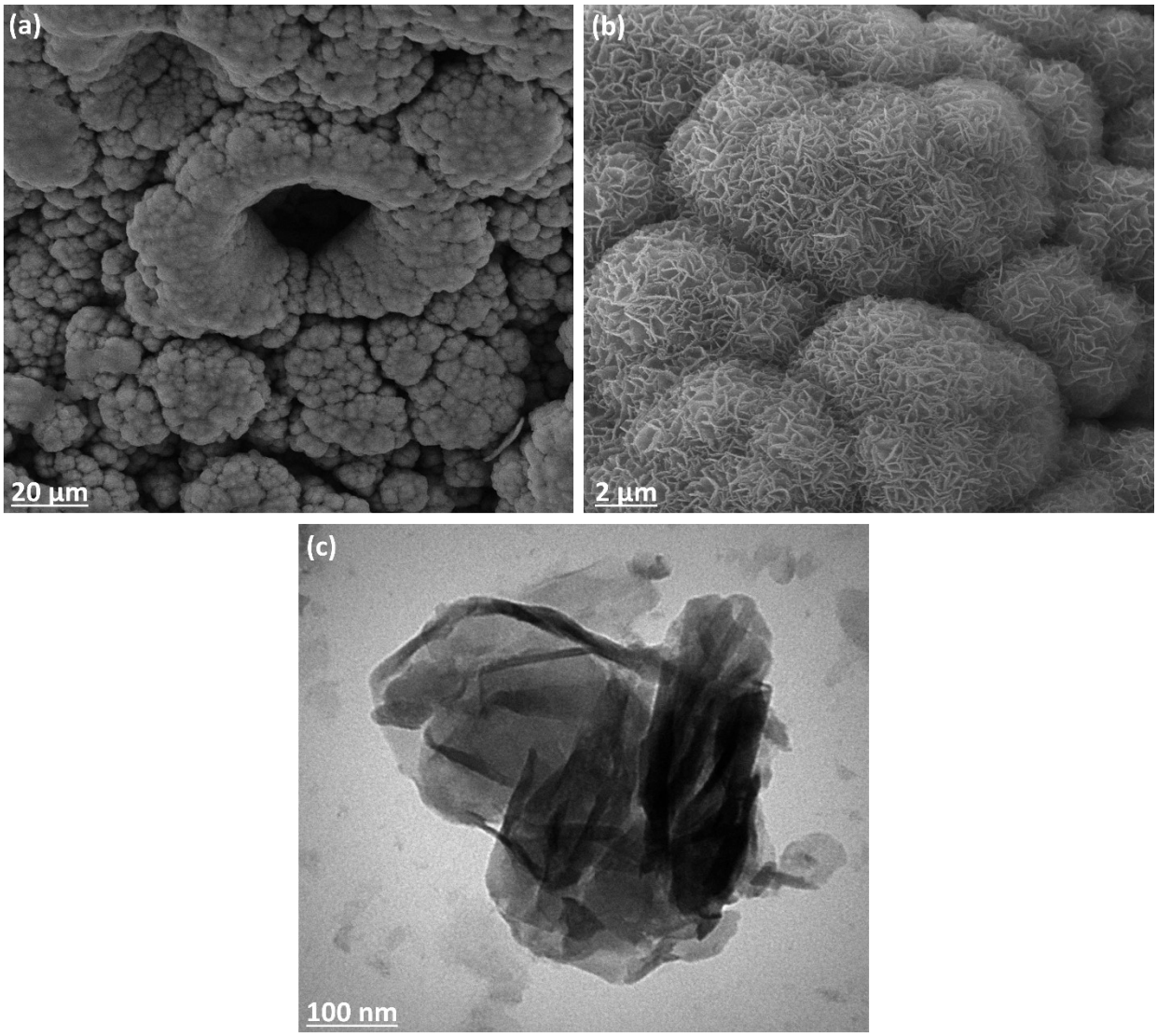

Figure. S11. FESEM (a), (b), and TEM (c) images of NiCoMn/NF After HER stability.

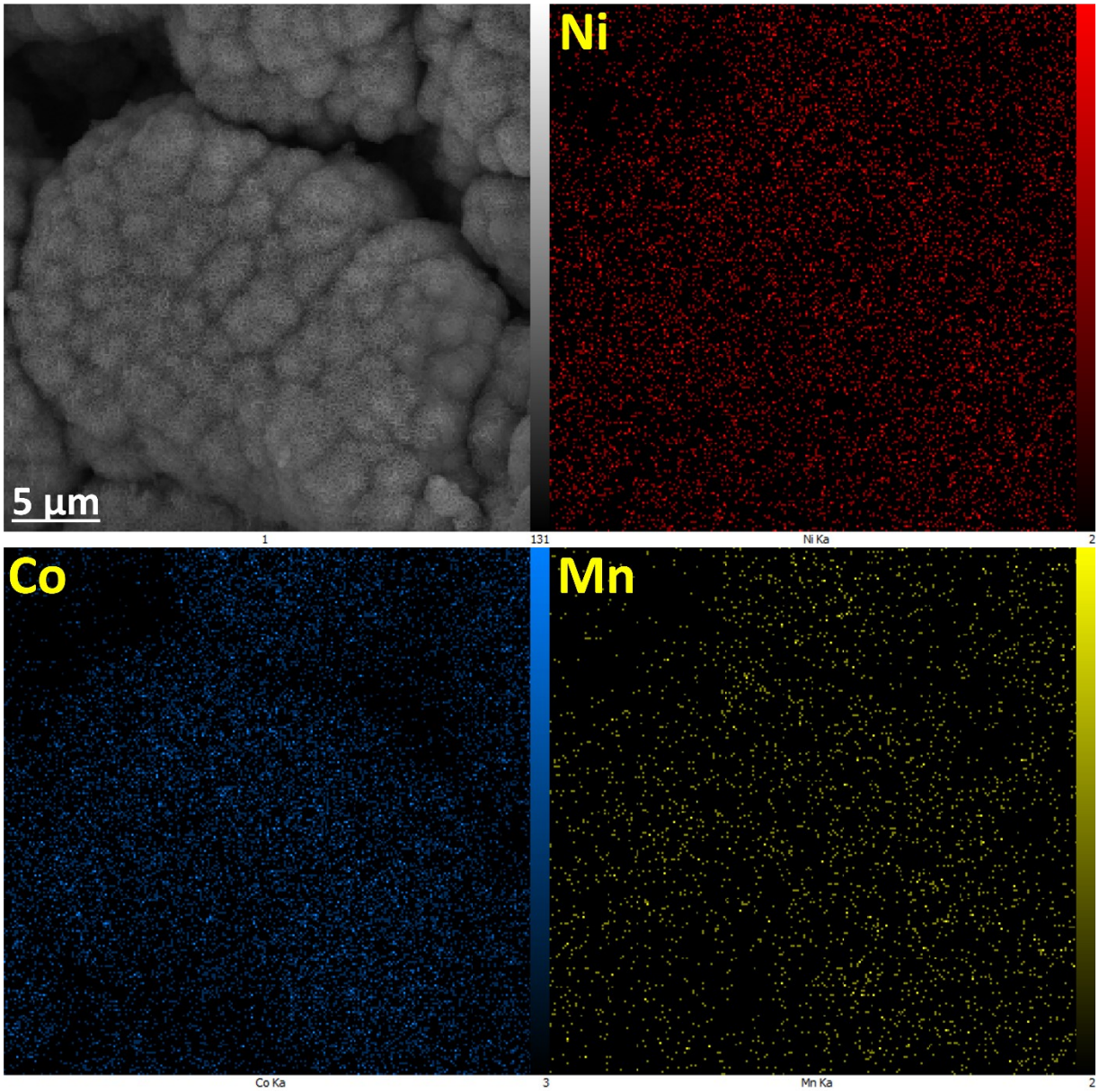

Figure. S12. EDS-elemental mapping of NiCoMn/NF electrode post-HER (1.0 M KOH), Ni (red), Co (blue), and Mn (yellow).

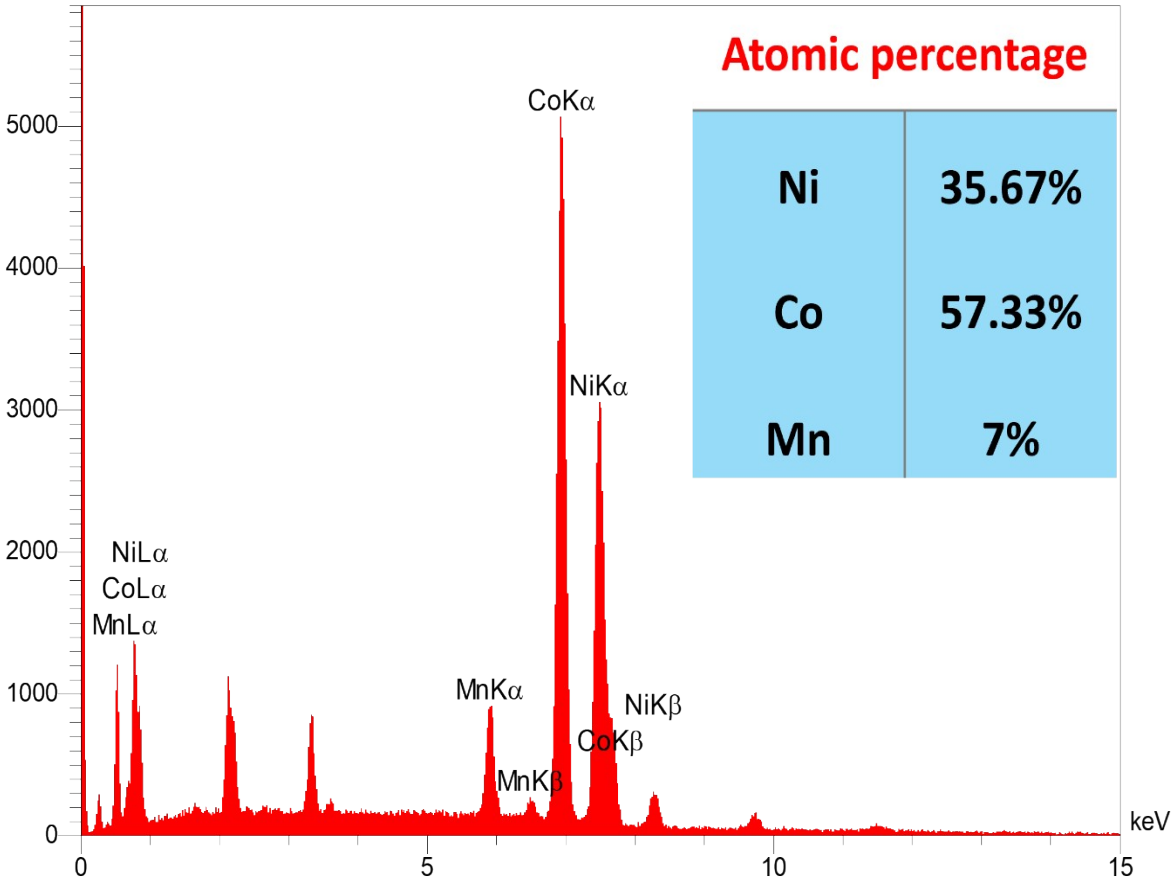

Figure. S13. Post-HER (1.0 M KOH) EDS spectra related to the NiCoMn/NF sample.

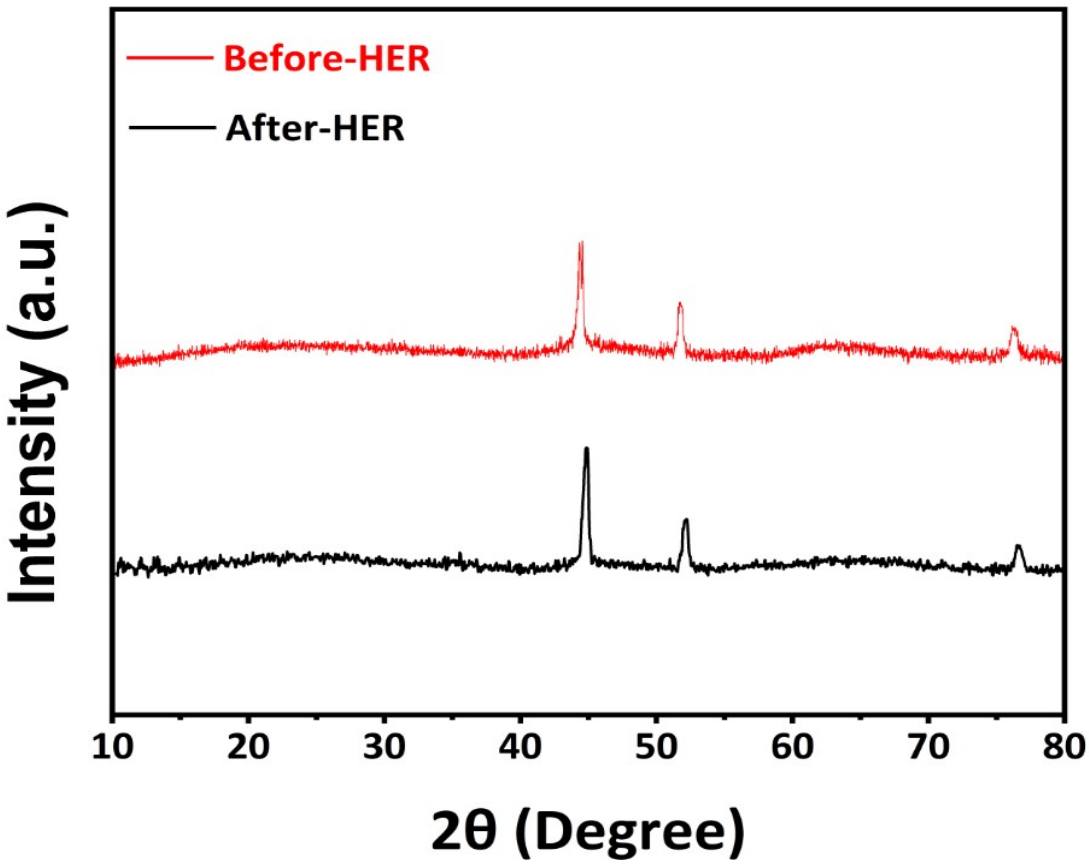

Figure. S14. XRD pattern of NiCoMn/NF before and after-HER.

Table. S3. The atomic percentages for NiCoMn/NF electrocatalyst before and after HER stability tests obtained from FESEM-EDS and ICP-OES.

samples	Ni (%) ICP - OES	Ni (%) FESEM - EDS	Co (%) ICP - OES	Co (%) FESEM - EDS	Mn (%) ICP - OES	Mn (%) FESEM - EDS
NiCoMn/NF	50.05	50.83	44.86	44.13	4.97	5.04
NiCoMn/NF after HER stability test	46.39	37.67	48.15	55.33	5.46	7.00

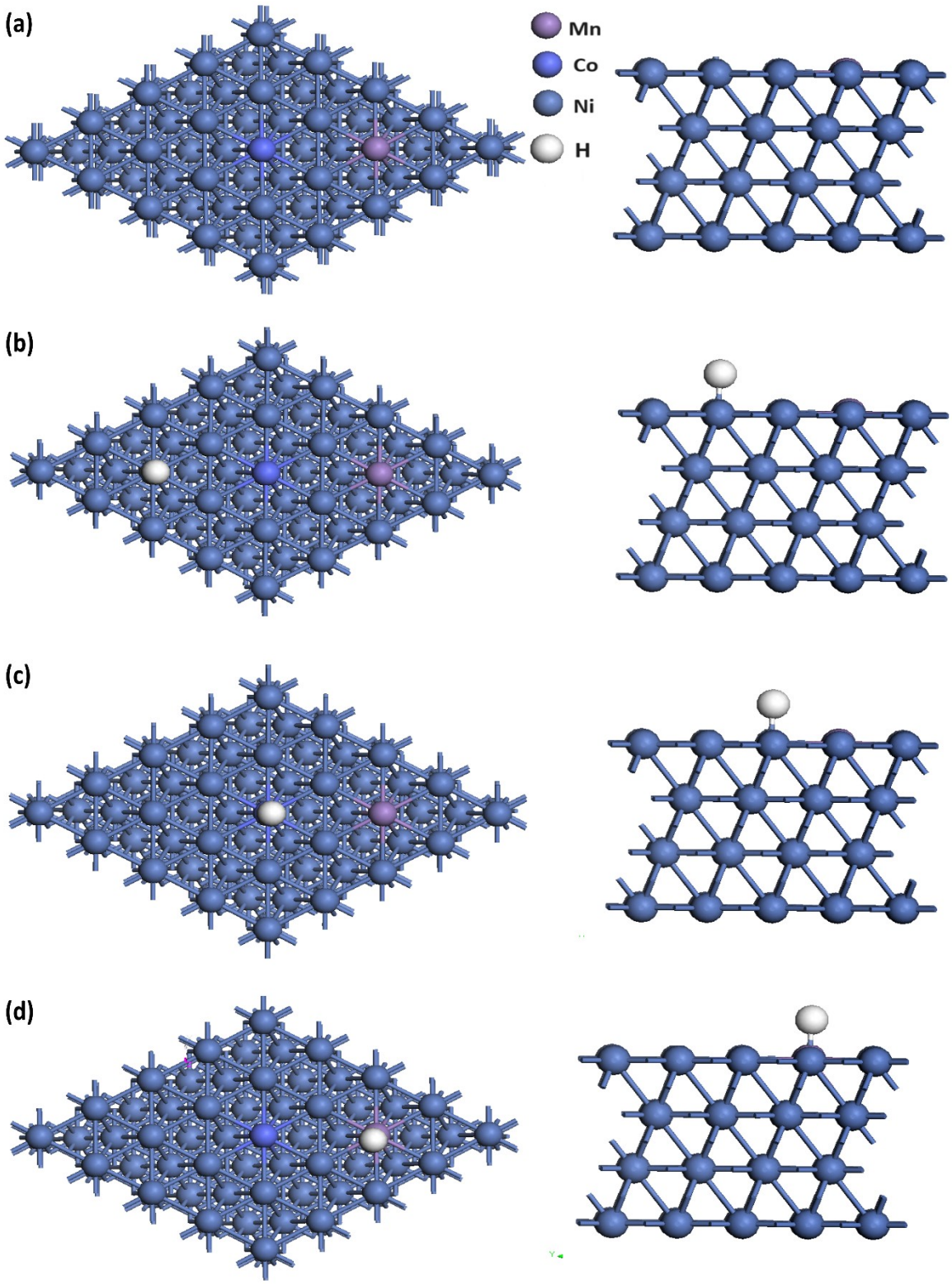

Figure. S15. Optimized structures showing (a) NiCoMn alloy and attachment of H on (b) NiCoMn -Ni, (c) NiCoMn -Co, (d) NiCoMn –Mn in HER.

References

1 M. Sarno, E. Ponticorvo and D. Scarpa, *Electrochem commun*, 2020, **111**, 106647.

2 S. Liu, E. Zhang, X. Wan, R. Pan, Y. Li, X. Zhang, M. Su, J. Liu and J. Zhang, *Sci China Mater*, 2022, **65**, 131–138.

3 F. Qin, Z. Zhao, M. K. Alam, Y. Ni, F. Robles-Hernandez, L. Yu, S. Chen, Z. Ren, Z. Wang and J. Bao, *ACS Energy Lett*, 2018, **3**, 546–554.

4 N. Lotfi and G. B. Darband, *J Electrochem Soc*, 2022, **169**, 096508.

5 G. Chen, T. Wang, J. Zhang, P. Liu, H. Sun, X. Zhuang, M. Chen, X. Feng, G. Chen, J. Zhang, H. Sun, X. Zhuang, X. Feng, T. Wang, P. Liu and M. Chen, *Adv Mater*, 2018, **30**, 1706279.

6 M. Khalid, A. M. B. Honorato, G. Tremiliosi Filho and H. Varela, *J Mater Chem A*, 2020, **8**, 9021–9031.

7 R. Biswas, S. G. Dastider, I. Ahmed, S. Barua, K. Mondal and K. K. Haldar, *J Phys Chem Lett*, 2023, **14**, 3146–3151.

8 S. E. Islam, D. R. Hang, C. Te Liang, K. H. Sharma, H. C. Huang and M. M. C. Chou, *ACS Appl Energy Mater*, 2023, **6**, 9543–9555.

9 Y. Chen, X. X. Zheng, X. Y. Huang, A. J. Wang, Q. L. Zhang, H. Huang and J. J. Feng, *J Colloid Interface Sci*, 2020, **559**, 206–214.

10 G. Wang, W. Chen, G. Chen, J. Huang, C. Song, D. Chen, Y. Du, C. Li and K. K. Ostrikov, *Nano Energy*, 2020, **71**, 104637.

11 H. Rajan, S. Anantharaj, J. K. Kim, M. J. Ko and S. C. Yi, *J Mater Chem A*, 2023, **11**, 16084–16092.

12 K. K. Joshi, P. M. Pataniya, G. Bhadu and C. K. Sumesh, *Int J Hydrogen Energy*, 2023, **48**, 7260–7272.

13 H. Y. Chen, H. J. Niu, Z. Han, J. J. Feng, H. Huang and A. J. Wang, *J Colloid Interface Sci*, 2020, **570**, 205–211.

14 W. Hong, S. Sun, Y. Kong, Y. Hu and G. Chen, *J Mater Chem A*, 2020, **8**, 7360–7367.

15 B. Jiang, Y. Sun, F. Liao, W. Shen, H. Lin, H. Wang and M. Shao, *J Mater Chem A*, 2017, **5**, 1623–1628.

16 B. Jiang, L. Yang, F. Liao, M. Sheng, H. Zhao, H. Lin and M. Shao, *Nano Res*, 2017, **10**, 1749–1755.

17 A. Mahmood, H. Lin, N. Xie and X. Wang, *Chem Mater*, 2017, **29**, 6329–6335.

18 K. E. Salem, A. A. Saleh, G. E. Khedr, B. S. Shaheen and N. K. Allam, *Energy Environ Mater*, 2023, **6**, e12324.

19 N. Chauhan, H. W. Choi, M. Kumar and D. H. Yoon, *Electrochim Acta*, 2023, **460**, 142634.

20 C. Chen, T. Song, H. Shang, Q. Liu, M. Yuan, C. Wang and Y. Du, *Int J Hydrogen Energy*, 2020, **45**, 26920–26928.

21 Y. C. Shi, T. Yuan, J. J. Feng, J. Yuan and A. J. Wang, *J Colloid Interface Sci*, 2017, **505**, 14–22.

22 T. Chao, X. Luo, W. Chen, B. Jiang, J. Ge, Y. Lin, G. Wu, X. Wang, Y. Hu, Z. Zhuang, Y. Wu, X. Hong and Y. Li, *Angew Chemie Int Ed*, 2017, **56**, 16047–16051.

23 M. Rafei, X. Wu, A. Piñeiro Garcia, V. Miranda la Hera, T. Wågberg and E. Gracia-Espino, *Adv Mater Interfaces*, 2022, **9**, 2201214.

24 S. Li, Q. Zhang, J. Sun and J. Guan, *Mater Today Energy*, 2020, **17**, 100464.

25 J. Tourneur, C. Lagrost and B. Fabre, *Adv Energy Sustain Res*, 2024, **5**, 2300133.